

# Autonomous Head-to-Head Racing in the Indy Autonomous Challenge Simulation Race

Gabriel Hartmann<sup>1,2</sup>, Zvi Shiller<sup>1</sup>, and Amos Azaria<sup>2</sup>

**Abstract**—This paper describes Ariel Team’s autonomous racing controller for the Indy Autonomous Challenge (IAC) simulation race [1]. IAC is the first multi-vehicle autonomous head-to-head competition, reaching speeds of 300 km/h along an oval track, modeled after the Indianapolis Motor Speedway (IMS).

Our racing controller attempts to maximize progress along the track while avoiding collisions with opponent vehicles and obeying the race rules. To this end, the racing controller first computes a race line offline. Then, it repeatedly computes online a small set of dynamically feasible maneuver candidates, each tested for collision with the opponent vehicles. Finally, it selects the maneuver that maximizes progress along the track, taking into account the race line.

The maneuver candidates, as well as the predicted trajectories of the opponent vehicles, are approximated using a point mass model. Despite the simplicity of this racing controller, it managed to drive competitively and with no collision with any of the opponent vehicles in the IAC final simulation race.

## I. INTRODUCTION

The Indy Autonomous Challenge (IAC) is an international competition, organized by Energy System Network (ESN), intended to promote the development of algorithms driving under challenging conditions. The IAC of 2020-2021 is the world first multi-vehicle, high speed, head-to-head autonomous race held on the Indianapolis Motor Speedway (IMS). Over 30 teams from universities around the globe participated in the challenge. The competition is carried out

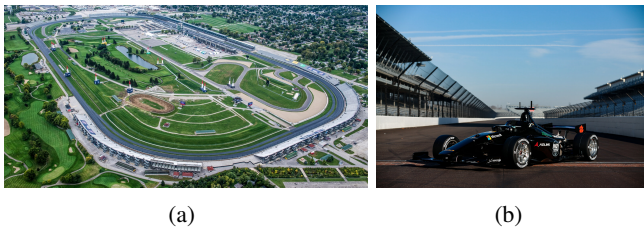


Fig. 1: (a) The Indianapolis Motor Speedway (b) the AV-12 autonomous race car.

in two stages: a simulation race, and a real race on IMS with the Dallara AV-21, which reaches speeds of up to 300 km/h

This research was supported, in part, by the Ministry of Science & Technology, Israel.

This work has been submitted to the IEEE for possible publication. Copyright may be transferred without notice, after which this version may no longer be accessible.

<sup>1</sup> Department of Mechanical Engineering and Mechatronics, Ariel University, Israel

<sup>2</sup> Department of Computer Science, Ariel University, Israel  
gabrielh@ariel.ac.il, shiller@ariel.ac.il,  
amos.azaria@ariel.ac.il

and is based on a race car of the Indy Lights series. The official simulator for the IAC is the Ansys VRXPERIENCE simulator [2], which simulates the AV-21 dynamics and the IMS track (see Fig. 2). Prior to the competition, all teams were required to demonstrate autonomous control of a real vehicle (see [3] for the demonstration submitted by our team). During the development period, which lasted 16 months, there were three testing events that gradually led to the final simulation race. The simulation race is composed of four parts: solo laps, in which all vehicles drive alone; safety tests that validate the ability of each vehicle to avoid collisions and obey the race rules; semi-finals, in which the place in the grid is set according to the solo lap times; and the final race.



Fig. 2: The VRXPERIENCE simulator used for the simulation race.

### A. Challenges of autonomous racing

Autonomous racing has unique challenges, emanating from the unique properties of the race vehicle, its extreme speeds, and the competitive nature of the driving.

*a) Extreme speeds:* Racing speeds coupled with limited frequencies of the sensor readings lead to state updates at large distance intervals compared to the vehicle size and the distance between neighboring vehicles. Furthermore, driving near the vehicle’s performance envelope at close proximity to neighboring vehicles leaves little room for correction and hence requires high fidelity prediction of the behavior of the opponent vehicles.

*b) Competitive driving:* Competitive driving forces the competitors to race at close proximity to opponent vehicles and to often block other vehicles from passing. As a result, the time difference between the leading teams is in the order of a fraction of a second. This in turn forces all competitors to drive on the performance envelop of the vehicle and the driver, leaving little room for safety. Although the goal is to win the race, in our opinion, especially at the first time that such head-to-head race is taking place, safer behavior and larger safety margins should be preferred over pushing the performance to the limits.

c) *Aerodynamics forces*: The aerodynamics of a race car has two main effects: a down-force that increases the tire grip and lets the car reach a lateral acceleration of over  $2.5g$ , which allows driving at maximal speeds along an oval track. The second effect is a slipstream, or draft, which reduces the drag on the following vehicle. This allows vehicles of identical dynamics to overtake each other. The racing rules [4] are derived from the rules used in human-driven races. An important principle is that an overtaking vehicle is responsible to avoid collision with a vehicle that is moving on its race line, while the overtaken vehicle is expected to maintain its own race line. In the simulated race, a vehicle is disqualified if it leaves the track.

### B. Related Work

Unlike the IAC which is a head-to-head autonomous race, other autonomous racing competitions of full-size vehicles, traveling at high speeds, such as the formula student challenge [5] or Roborace [6], focus mainly on solo racing. In solo racing, since it is not required to attend to other vehicles, one must drive the vehicle along a time-optimal race line at time-optimal speeds. This was achieved using model predictive control (MPC) [7], [8] and reinforcement learning [9], [10].

Racing against multiple vehicles is more challenging than solo racing as it requires the online prediction of the trajectories of the neighboring vehicles, and the planning of a dynamically safe avoidance maneuver. A survey of early prediction methods is presented in [11]. An early approach to trajectory prediction uses Kalman filter assuming a constant velocity and acceleration [12]. A more recent approach uses recurrent neural networks to predict multi modal distribution of future trajectories [13].

Two main approaches for driving in dynamic environments have emerged: one generates online control commands, whereas the other tracks a selected trajectory.

Online control commands can be generated using MPC to repeatedly optimize a forward trajectory, while accounting for geometric constraints, moving opponent vehicles, and ego-vehicle dynamics. MPC was demonstrated in [8] to avoid static obstacles, and in [14] to drive competitively in a head-to-head race with two vehicles. Another method to online generate control commands is based on the concept of Velocity Obstacles (VO), which maps static and dynamic obstacles (e.g. opponent vehicles) to the velocity space of the ego vehicle [15], [16]. This allows an efficient selection of a collision free velocity that avoids an arbitrary number of vehicles.

The second approach for driving in dynamic environments divides the driving task into two simpler sub-tasks: first plan a trajectory, then track this trajectory using a tracking controller. The trajectory planner can be simplified by using a simple dynamic model to compute a collision free trajectory. The tracking controller then tracks the trajectory without considering the obstacles.

The trajectory can be computed using a graph search in a spatiotemporal lattice [17], in a spatial lattice [18], or by an

RRT\* (Rapid Random Tree) search [19].

Trajectory tracking can be accomplished using simple geometric controllers or more complex controllers that takes the vehicle dynamics directly into account [20].

### C. This paper

The autonomous racing controller, developed by “Ariel Team”, was developed under the underlying principle, which must guide all developers of autonomous vehicles, that emphasizes safety over performance. To this end, our controller attempted to avoid collisions, even if the race rules placed the responsibility to avoid the collision on the opponent vehicle.

The racing controller is based on a repeated search for the locally best maneuver that avoids collisions with opponent vehicles, attempts to follow the globally optimal race line, and obeys the race rules.

A set of local maneuvers are generated at  $25Hz$ , using a point mass model from the current state to a small set of discrete points along the track. At each step, the selected maneuver is tracked using pure-pursuit and a proportional velocity controller. Our approach resembles the approach used in [21], [22] for urban driving.

It is interesting to note that despite its simplicity, our controller demonstrated competitive driving while overtaking other vehicles, staying within a close range of the leading vehicle, and not being involved in any collision throughout the race. Furthermore, our vehicle maintained the 3<sup>rd</sup> place for a major part of the semi-finals and the finals. We ended up getting off the track, with 3 laps to go, while avoiding a vehicle that entered our safety bound. This placed us 6<sup>th</sup> in the final simulation race.

## II. SOFTWARE ARCHITECTURE

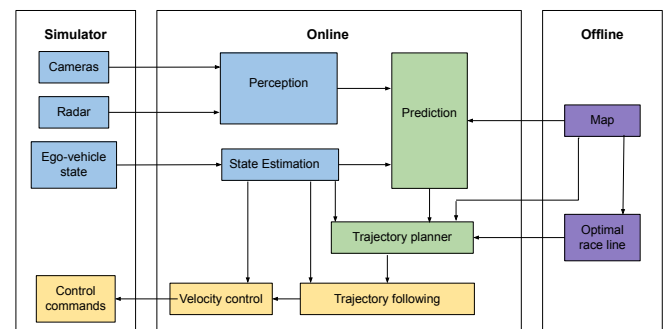


Fig. 3: Software Architecture.

The software architecture is shown schematically in Fig 3. For a given track map, we first compute an optimal race line, offline, which will serve us throughout the race. The data from the cameras and radars provide the position and velocity of the surrounding opponent vehicles, and additional simulated sensors provide the ego-vehicle state e.g., position and velocity. These data, together with the map and the optimal race line, are used by the prediction module to repeatedly predict future trajectories of the opponent vehicles. The same information is used by the trajectory

planner to plan an optimal local maneuver for the ego-vehicle. This maneuver serves as an input to the trajectory-following controller, which computes the desired linear and angular velocities of the ego-vehicle. The linear and angular velocities are controlled by the velocity controller which outputs the steering, throttle and brake commands.

### III. COMPUTING THE OPTIMAL RACE LINE

The optimal race line is a time optimal trajectory computed offline, based on the track geometry and vehicle dynamics.

The IMS is an oval track, 2.5 miles (4,023 m) long, as depicted in Fig. 4a.

We computed the optimal race line using an open-source trajectory optimization software, [23]. The optimal race line, typically maximizes the radius of curvature by entering the corner on the outside boundary of the track, passing through the apex on the inner boundary, to the exit point on the outside boundary, as shown in Fig. 4.

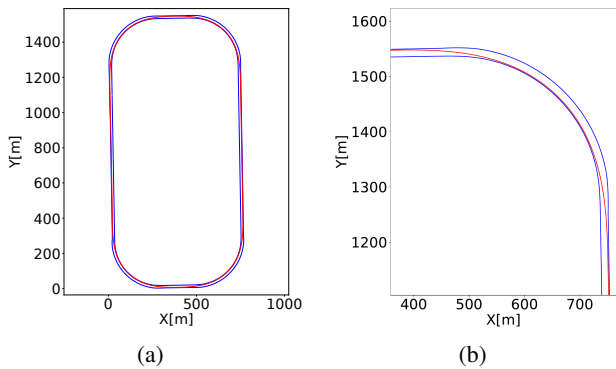


Fig. 4: (a) The IMS track. (b) The optimal race line around a corner of the track.

### IV. ONLINE TRAJECTORY PLANNING

The online trajectory planner computes a collision free trajectory at 25 Hz with a planning horizon of 200 m. It is used as a reference for the trajectory following controller (see Section V). The planner first generates 8 dynamically feasible maneuver candidates, then selects the best candidate that maximizes progress along the path and avoids collision with the opponent vehicles. Since the planning horizon of is limited to 200 m, and the typical driving speed is over 80 m/s, the time horizon is less than 3 seconds. The small number of maneuver candidates, generated at 25Hz, and the short time horizon, sufficiently span the set of options of possible feasible maneuvers, as demonstrated in the simulation runs presented later in Section VI.

#### A. Coordinate system

An ego-vehicle- and road-aligned coordinate system is used for planning, such that  $x$  axis is tangent to the left track boundary and the  $y$  axis is normal to track. The position of the ego-vehicle is denoted as  $(x_e, y_e)$ ; since the coordinate system is aligned with the ego-vehicle, the ego-vehicle is always located at  $x_e = 0$ .  $y_e$  represents the ego-vehicle's normal shift from the left boundary. (see Fig. 5).

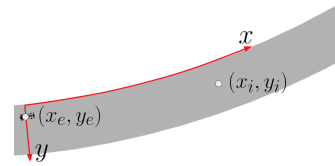


Fig. 5: Road-aligned coordinate system.

In our coordinate system for every point  $(x_i, y_i)$ ,  $|x_i|$  represents the distance from the ego-vehicle along the track (a negative  $x_i$  represents a point behind the ego-vehicle), and  $y_i$  represents the shift from the boundary regardless of the track shape and the ego-vehicle's location.

#### B. Computing a trajectory between two point

In this section, we explain how two trajectory points (a start point and a goal point) are connected to form a trajectory based on the time-optimal motion of a point-mass model. This method is used for opponent vehicles trajectories predictions and planning maneuver candidates for the ego-vehicle.

Let  $p_s = \{x_0, y_0, \dot{x}_0, \dot{y}_0\}$  be the start point, and let  $p_g = \{x_g, y_g, \dot{x}_g, \dot{y}_g\}$  be the goal point. We plan a trajectory  $C(t) = \{x(t), y(t), \dot{x}(t), \dot{y}(t)\}$ ,  $t \in [0, T]$  that connects the start point with the goal point, i.e.  $C(0) = p_s$  and  $C(T) = p_g$ . For composing the trajectory we first assume that  $\dot{x}_s = \dot{x}_g$ , i.e. the starting velocity (in the  $x$  axis) equals the goal velocity, and later re-adjust the velocity. Therefore, the final time  $T$  is:

$$T = \frac{x_g - x_0}{\dot{x}_0}.$$

$C$  is created by applying a bang-bang lateral force with a single switch point on a point mass  $m$ , similar to [24].

Let  $F_y$  be a force, such that:

$$F_y = \frac{-\sqrt{2A} - T(\dot{y}_g + \dot{y}_0) + 2(y_g - y_0)}{T^2 m}$$

where,  $A = (T^2(\dot{y}_0^2 + \dot{y}_g^2) - 2T(y_g - y_0)(\dot{y}_g + \dot{y}_0) + 2(y_g - y_0)^2)$ . The bang-bang lateral force is applied in one direction until a switching time,  $T_s$ , and then the force is applied in the opposite direction, i.e.,  $F_y$  is applied for  $t = [0, T_s]$  and  $-F_y$  is applied for  $t = (T_s, T]$ .

$$T_s = \frac{m(\dot{y}_g - \dot{y}_0) + F_y T}{2F_y}$$

Finally,  $C(t)$  is computed for  $t \in [0, T]$  by:

$$\begin{aligned} x(t) &= \dot{x}_0 t \\ y(t) &= \begin{cases} \dot{y}_0 t + \frac{1}{2} \frac{F_y}{m} t^2 & t < T_s \\ \dot{y}_0 t - \frac{1}{2} \frac{F_y}{m} t^2 & t > T_s \end{cases} \\ \dot{x}(t) &= \dot{x}_0 \\ \dot{y}(t) &= \begin{cases} \dot{y}_0 + \frac{F_y}{m} t & t < T_s \\ \dot{y}_0 + \frac{F_y}{m} (2T_s - t) & t > T_s \end{cases} \end{aligned}$$

Fig. 6 illustrates an example of a trajectory that connects two points.

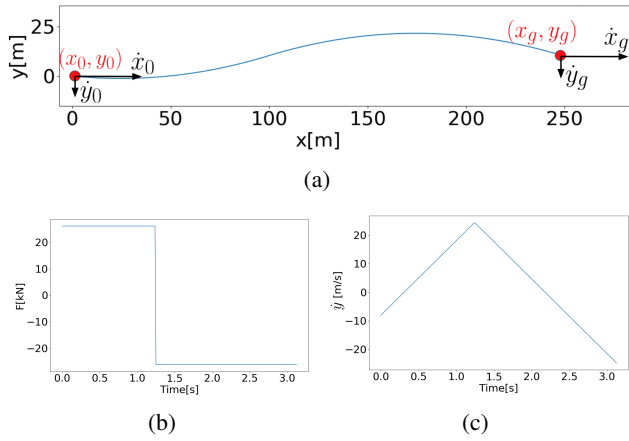


Fig. 6: A trajectory between given start and goal points. (a) Force  $F_y$  is applied on mass  $m$  to create a continuous trajectory between the points. (b) The lateral force  $F_y$  profile and (c) the lateral velocity  $\dot{y}(t)$ .

### C. Opponents vehicles' trajectory prediction

An important part of motion planning in a dynamic environment and especially in racing is to predict the future positions and velocities of all the other vehicles surrounding the ego-vehicle. Therefore, we develop a prediction module, which given opponent vehicle state  $s$  that contains position  $x_o, y_o$ , velocity  $\dot{x}_o, \dot{y}_o$  and angular velocity  $\omega_o$ , predicts the future trajectory  $J(t) = \{x(t), y(t), \dot{x}(t), \dot{y}(t)\}$  up to a predefined time horizon  $T_{max}$ , which we set to 3 seconds.

Our prediction module first predicts other vehicles future trajectory by assuming that they retain their current steering and then updates its prediction according to the track boundaries. Namely, for a given opponent vehicle, we first predict a future trajectory,  $\hat{J}$ , that keeps a constant curvature  $\kappa$ , which we approximate by:  $\kappa = \frac{\omega_o}{\|\dot{x}_o + \dot{y}_o\|}$ . However, it is expected that the opponent vehicle will consider the track boundaries and will avoid exceeding them. Therefore, our prediction module also takes the track boundaries into account and uses the following method. Let  $(\hat{x}, \hat{y})$  be the first position on  $\hat{J}$  in which the opponent vehicle approaches one of the boundaries and is only a distance of  $d_{min}$  from it. We define three trajectory points,  $p_0, p_1$  and  $p_2$  as described hereunder, where each trajectory point is composed of  $p_i = \{x_{p_i}, y_{p_i}, \dot{x}_{p_i}, \dot{y}_{p_i}\}$ ; the prediction module connects them by a point mass maneuver as explained in Section IV-B. The first trajectory point,  $p_0$  is derived from the opponent vehicle's current state  $s$ , such that  $x_{p_0} = x_o, y_{p_0} = y_o, \dot{x}_{p_0} = \dot{x}_o$ , and  $\dot{y}_{p_0} = \dot{y}_o$ . The second trajectory point,  $p_1$ , is based on  $(\hat{x}, \hat{y})$ , but we assume that the opponent vehicle will not increase its curvature; therefore, we assume that  $\hat{y}$  will be reached later on, by a predefined factor,  $k$ . That is,  $x_{p_1} = (\hat{x} - x_o)k, y_{p_1} = \hat{y}, \dot{x}_{p_1} = \dot{x}_o, \dot{y}_{p_1} = 0$ . The third trajectory point,  $p_2$  retains the lane parallel to the boundary up to  $T_{max}$ , i.e.,  $x_{p_2} = \dot{x}_o T_{max}, y_{p_2} = \hat{y}, \dot{x}_{p_2} = \dot{x}_o$ , and  $\dot{y}_{p_2} = 0$ . Examples of predicted trajectories are shown in Fig. 7.

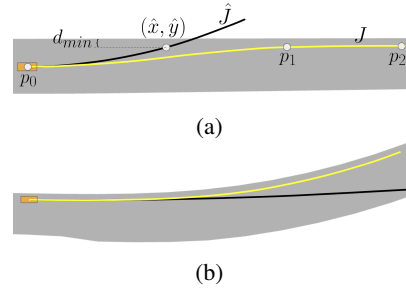


Fig. 7: Predicted trajectories of an opponent vehicle (marked as an orange bounding box). Black indicates constant curvature trajectory  $\hat{J}$ , and yellow indicates  $J$ , which considers the track boundaries. In (a)  $\hat{J}$  exceeds track boundaries; therefore, a lane-changing trajectory is predicted by  $J$ ; in (b) although the vehicle drives on a straight line, a lane-keeping trajectory is predicted by  $J$ .

We note that our method for trajectory prediction assumes that other vehicles follow a smooth motion profile. The justification for this assumption relies on the fact that in time horizon, when traveling at high velocity, and since the racing rules prohibit sudden changes of racing lines, other vehicles are likely to continue their motion profiles.

### D. Creating maneuver candidates

The online trajectory planner plans a set of dynamically feasible maneuver candidates and selects one of them according to multiple criteria, as follows.

1) *Lane change maneuver*: Given ego-vehicle's state  $s_e = \{x_e, y_e, \dot{x}_e, \dot{y}_e\}$  and a lateral target  $\hat{y}$ , which defines the target lane, the planner module creates a lane change maneuver,  $C^{\hat{y}}$ , by connecting the following three trajectory points,  $q_i = \{x_{q_i}, y_{q_i}, \dot{x}_{q_i}, \dot{y}_{q_i}\}$ , where  $i \in \{0, 1, 2\}$ , as described in Section 8.

$q_0$  is derived from ego vehicle's current state  $s_e$ , such that  $q_0 = s_e$ . The second point defines the lateral distance of the desired lane  $\hat{y}$  and the longitudinal lane-changing distance that depends linearly on the lateral changing distance  $(\hat{y} - y_e)$  by a predefined factor  $b$  and predefined constant  $c$ . That is,  $x_{q_1} = \{(\hat{y} - y_e)b + c, y_{q_1} = \hat{y}, \dot{x}_{q_1} = \dot{x}_e, \dot{y}_{q_1} = 0\}$ . The third trajectory point,  $q_2$  retains the lane parallel to the boundary up to a maximal longitudinal distance  $x_{max}$ , i.e.,  $x_{q_2} = x_{max}, y_{q_2} = \hat{y}, \dot{x}_{q_2} = \dot{x}_e$ , and  $\dot{y}_{q_2} = 0$ . Fig. 8a illustrates a lane change maneuver.

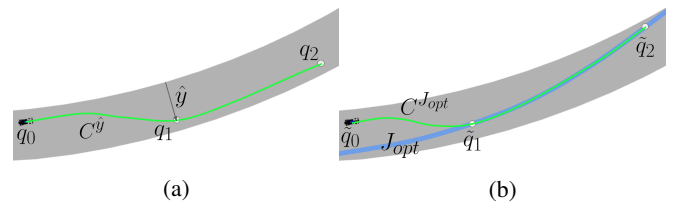


Fig. 8: Illustration of the maneuver candidates planning: (a) lane change maneuver and (b) a maneuver to the optimal race line.



We define  $N$  equally spaced lanes, with zero width, which represent potential  $\hat{y}$  values. The first and last lane are far enough from the boundaries to allow a vehicle to follow them safely. Our planner generates  $N$  lane change maneuvers, one for each defined lane. Let  $\mathbf{M}'$  be the set of all lane change maneuvers. More formally,

$$\mathbf{M}' = \bigcup_{i=0}^{N-1} C^{\hat{y}_i}, \quad \hat{y}_i = d_{min} + \frac{w - 2d_{min}}{N - 1}i$$

where  $d_{min}$  is the minimal distance to keep from track boundaries. The width of the track in most segments is 14 m; we set  $N = 7$  to achieve a distance between lanes, that is close to the vehicles width (2 m).

2) *Maneuver to the the optimal race line:* In addition to these lane-changing maneuvers, we plan a maneuver  $C^{J_{opt}}$ , which smoothly merges with the optimal race line  $J_{opt}$ . We define the following three trajectory points  $\tilde{q}_i = \{x_{\tilde{q}_i}, y_{\tilde{q}_i}, \dot{x}_{\tilde{q}_i}, \dot{y}_{\tilde{q}_i}\}$ , where  $i \in \{0, 1, 2\}$ .

The first trajectory point  $\tilde{q}_0 = s_e$ ; the second,  $\tilde{q}_1 \in J_{opt}$  such that  $\{(y_{\tilde{q}_1} - y_e)b + \tilde{c} = x_{\tilde{q}_1}$ , where  $\tilde{b}$  and  $\tilde{c}$  are predefined constants. Finally,  $\tilde{q}_2 \in J_{opt}$  such that  $x_{\tilde{q}_2} = x_{max}$ . See Fig. 8b).

The full set of the maneuver candidates is  $\mathbf{M} = \mathbf{M}' \cup C^{J_{opt}}$ , as shown in Fig. 9.

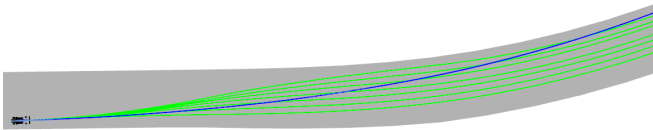


Fig. 9: Example of 7 lane-changing maneuvers (green) and a maneuver that merges with the optimal race line (blue).

### E. Velocity re-planning

Although the maneuver candidates  $\mathbf{M}$  and the predicted trajectories of the opponent vehicle include velocities in addition to positions, these velocities were only used to define the direction of the paths and to estimate the lateral forces on the vehicle. Therefore, the velocity profiles are re-planned to more accurately represent the future motion, by assuming that the vehicles accelerate along the trajectories until reaching the maximal velocity. This is possible since our planned trajectories approximate the vehicle dynamics and thus, allow maintaining maximal velocity—without losing control—when following them.

### F. Collision

To avoid a collision, due to the uncertainty inherent to our problem, we define a safety bound around the vehicle. We attempt not only to avoid a collision with another vehicle but also to avoid any overlap between the safety bounds around both vehicles. We use a rectangular safety distance; we define the longitudinal safety bound as 0.3 of the vehicle length both front and rear, and the lateral safety distance as 0.5 of the vehicle width, right and left. This results in keeping a

longitudinal safety bound of 0.6 of a vehicle and a lateral safety bound of an entire width of a vehicle. We note that, while a circular safety bound is more convenient because the yaw angles of the vehicles are indifferent, since the length of the race car is more than double its width, a circular safety bound would not fit well to the vehicle's shape. Since the slip angles are small, the yaw angles, of the vehicles is approximated by the angle of vehicle's velocity vector.

Two trajectories  $C_1$  and  $C_2$  describe a collision if there exists some  $t$  that the safety bounds of both associated vehicles at time  $t$  overlap. See Fig. 10 for an illustration.

A maneuver candidate is considered *free* if it does not collide with a predicted trajectory of any opponent vehicle. However, if an opponent vehicle is directly behind the ego-vehicle, and the ego-vehicle blocks it, our controller ignores it, since it is the opponent vehicle's clear responsibility to avoid a collision.

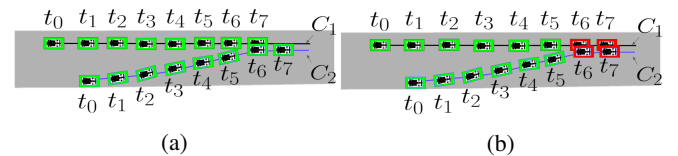


Fig. 10: Two trajectories describing the location of each vehicle and its safety bounds. In (a) the vehicles collide at time  $t_6$ ; in (b) the vehicles do not collide since the overlap of their safety bounds is at different times.

### G. Maneuver selection

Our planner considers all maneuver candidates that are free. Nevertheless, maneuver candidates that anticipated collision with a vehicle when proceeding at maximal velocity, are updated and their velocity is controlled so they do not collide, if possible (See Fig. 11).

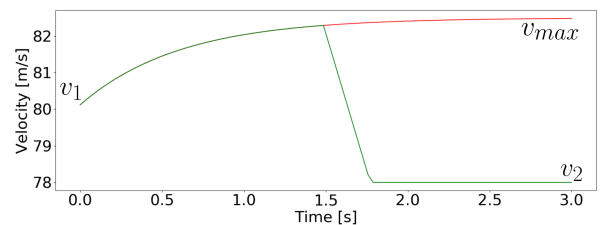


Fig. 11: Updating a maneuver candidate to become free by decelerating toward a blocking vehicle that drives at a velocity of  $v_2$  (green), instead of accelerating to the maximal velocity,  $v_{max}$  (red), and causing a collision.

If more than one maneuver is free, each maneuver is associated with a cost based on the following criteria; the maneuver with the lowest cost is selected.

1) *Maneuver expected time:* The time each maneuver is expected to take until reaching the planning horizon. For maneuver  $C$ , we use  $\mathcal{T}(C)$  to denote this time. For example, consider two maneuvers,  $C$  and  $C'$ , where  $C$  is shorter than  $C'$ , possibly because  $C'$  contains lane changing. If the

velocity along  $C$  and  $C'$  is equal, then  $\mathcal{T}(C) < \mathcal{T}(C')$ . However, if  $C$  is blocked by another vehicle which requires decelerating along that path to avoid the collision, it might be that  $\mathcal{T}(C) > \mathcal{T}(C')$ .

2) *Closest maneuver to the optimal trajectory*: The maneuver with the lowest expected time is only locally optimal since the short-horizon maneuver candidates are compared, but the global optimality is not considered. Incorporating global optimality into the maneuver candidates would require predicting and planning to an extended range, which would require extensive computing power and would raise uncertainty.

To partially account for global optimality, the planner prefers maneuvers that come close to the optimal race line, which is global optimal—without considering other vehicles. To encourage the selection of a maneuver that is the closest, among the free candidates, to the optimal race line, that maneuver obtains a reward  $R_o$ , which controls the trade-off between local time optimality and following the optimal race line. That is, for a maneuver  $C$ , let  $\mathcal{O}(C)$  be  $R_o$  if  $C$  is closest, among the free candidates, to the optimal race line, and 0 otherwise.

3) *Minimum change from the current trajectory*: The selected maneuver can change significantly at every time step when the optimality of two maneuver candidates is similar. To stabilize the planning, it is preferred, when possible, to keep the same maneuver, unless another maneuver is conspicuously better. Clearly, switching to a new maneuver is more severe if a switch has just occurred, but once some time has passed since the last switch, the controller should be more lenient towards another switch.

For a maneuver  $C$ , let  $\mathcal{K}(C)$  be  $R_k$  if  $C$  is the same maneuver as the maneuver that the vehicle currently drives on, and 0 otherwise.  $R_k$  drops with a linear decay rate  $R_d$  as long as the maneuver is followed, and is reset to its initial value  $R_{k_0}$  if the maneuver is switched.

Finally, the cost associated with each free maneuver  $C \in \mathcal{M}$  is  $\mathcal{T}(C) - \mathcal{O}_{opt}(C) - \mathcal{K}(C)$ . The maneuver with the minimal cost is selected. Fig. 12 a,b,c show examples of selected maneuvers.

#### H. Behavior when no maneuver is free

Situations in which none of the Maneuvers are free are unavoidable due to the unpredictable behavior of other vehicles and inaccurately modeled ego-vehicle dynamics. If none of the Maneuvers are free, the optimality criteria are not relevant and the only selection criterion is safety. To find the safest maneuver the planner finds the closest collision and selects a maneuver that is as far as possible from that collision (see an example at Fig. 12d).

## V. CONTROL

The control module outputs throttle, brake, and steering commands that drive the vehicle as close as possible to the selected maneuver.

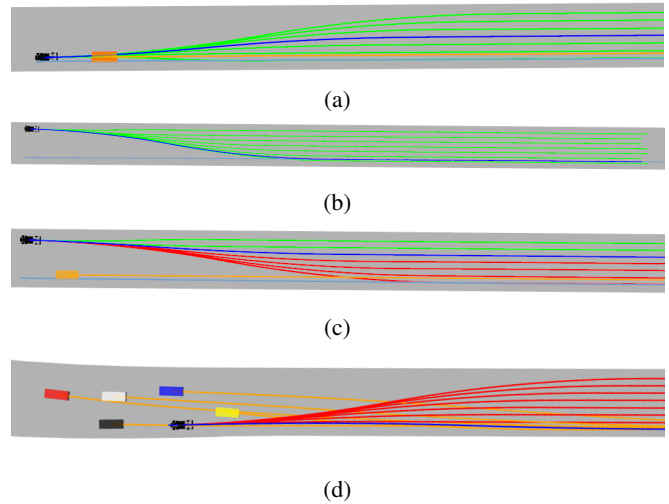


Fig. 12: Maneuver selection examples, green: free maneuvers, red: blocked maneuvers, blue: chosen maneuver. (a) The planner selects a minimum-time lane-changing maneuver because the current lane is blocked by another vehicle. (b) The planner prefers the longer maneuver because it returns to the optimal race line (shown in light-blue). (c) The planner selects a free maneuver that is the closest to the optimal race line. (d) None of the maneuver candidates are free, therefore the safest maneuver is chosen.

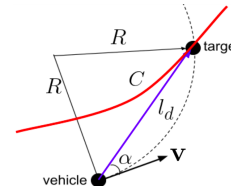


Fig. 13: Pure pursuit geometry.

#### A. Lateral control

The pure pursuit algorithm [25] is used to compute the desired angular velocity based on the current ego-vehicle's state and the selected maneuver, which is mapped to Cartesian coordinates. The pure pursuit algorithm pursues a target on the selected maneuver  $C$ . Let  $\mathbf{v}$  be the vector representing the ego-vehicle's velocity. The distance to the target is defined to be proportional to the vehicle's speed  $v = |\mathbf{v}|$  that is,  $l_d = vk_t$ , where  $k_t$  is a predefined constant. The angle between the velocity vector  $\mathbf{v}$  to the vehicle-target vector is denoted as  $\alpha$  (see Fig. 13). The desired angular velocity of the vehicle  $\omega_d$  is  $\frac{2v \sin \alpha}{l_d}$ . The desired angular velocity  $\omega_d$  is used as a reference for a proportional angular velocity controller that computes the steering command:  $\delta = (\omega_d - \omega)k_\omega$  where,  $\omega$  is the current angular velocity of the vehicle, and  $k_\omega$  is a proportional gain.

#### B. Longitudinal control

The desired speed  $v_d$  is provided by the selected maneuver, which is usually used as a reference for the longitudinal controller. However, when closely following a vehicle, we

modify the desired speed to be:  $v_d = v_f - (L_d - L)k_f$ , where  $v_f$  is the speed of the leading vehicle,  $L$  is the distance to the leading vehicle,  $L_d$  is the desired distance to keep, and  $k_f$  is a proportional gain. This modification allows smooth driving and keeping a constant distance from the leading vehicle. Fig. 14 illustrates a following scenario. Finally, the

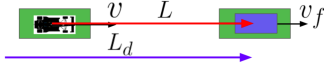


Fig. 14: Following a vehicle. The distance between the ego-vehicle and the vehicle ahead,  $L$ , is less than the predefined following distance,  $L_d$ ; therefore, the ego-vehicle will slow down, to increase  $L$ .

throttle and brake command  $u$  is computed by a proportional speed controller:  $u = (v_d - v)k_v$  where,  $k_v$  is a proportional gain.

## VI. EXPERIMENTS

### A. Simulation environment

The VRXPERIENCE simulator enables multi-vehicle head-to-head competitions, in which every vehicle is controlled by a separate controller. The sensors are simulated at 25 Hz and the ego-vehicle's state at 100 Hz, in simulator time. Each controller receives the ego-vehicle's state and the sensor data from the simulator, and sends back throttle, brake, and steering commands.

We used the pre-processed cameras and radars data from the simulator to obtain the position and linear and angular velocity of all vehicles in the sensors range. We based our controller on Autoware.auto [26] which is an open-source autonomous driving framework that uses ROS2 as middleware. The computation time of our algorithm is 20 milliseconds, on average, on an Intel Core i7 2.90 GHz CPU, which enables our algorithm to run in real-time. We note that running in real time was not a requirement for the simulation race, and therefore, it might be that other teams' algorithms required longer computation time. A video demonstrating our controller is available at [27].

### B. Simulation results

We tested our controller by competing between multiple instances of our controller. Clearly, every controller instance has information only from its vehicle sensors and operates independently from the other controllers. During our testings, all vehicles, which were using our controller, drove safely and respected the race rules; a collision or loss of control were never experienced. However, since different controllers can drive more aggressively and keep a smaller safety area, which is not observed when all controllers prioritize safety and drive more conservatively, testing with identical controllers does not ensure safe driving when competing against different controllers. Fig. 15 shows an example of the black vehicle's planner in a crowded 6-vehicle environment. Since following vehicles can exploit the slipstream, it is possible for them to overtake their leading vehicles. Indeed,

this phenomenon happened during our testing, despite all vehicles using the same controller. Fig. 16 demonstrates an overtake maneuver with 3 vehicles, all using our controller. At every corner, the black vehicle gains a small advantage over the blue vehicle until it successfully completes the overtaking maneuver.

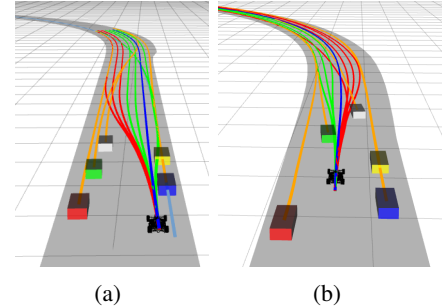


Fig. 15: Snapshots of planning in a crowded scenario with 5 opponent vehicles.

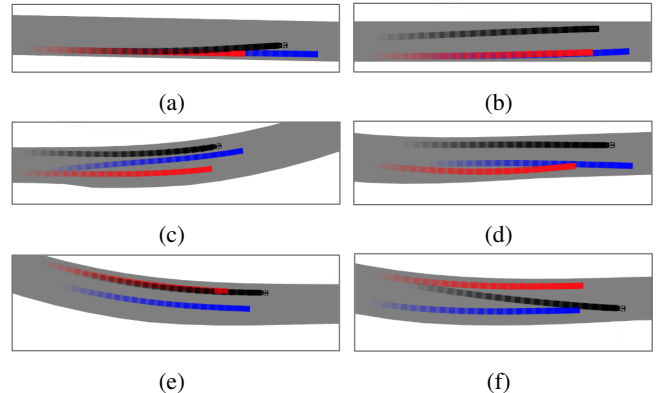


Fig. 16: An example of an overtake maneuver during a race; the trails represent the last 0.8 seconds. (a) The black vehicle initiates an overtake. (b) The black vehicle drives parallel to the blue and red vehicles. (c) The black vehicle prevents the blue vehicle from continuing on the optimal race line, i.e., reaching the apex. (d) The black vehicle gains a small advantage at the corner. (e) At the next corner, the blue vehicle is overtaken because it is forced to stay on the outside of the corner. (f) The black vehicle returns to the optimal race line.

### C. Results of the IAC simulation race

Only 16 teams reached the simulation race, as some of the teams were disqualified and some teams joined together. Our solo lap time, 51.968 seconds, placed us in 7<sup>th</sup> place; the first place finished only a 0.12 of a second (0.23%) before us. The average result was 53.041 seconds, placing us much closer to the first place than to the average. This result indicates the performance of the controller on the optimal race line. Only 10 teams passed the safety tests and were qualified to proceed to the semi-finals.

The semi-finals consist of a multi-ego, 10-lap competition. The remaining teams were split into two heats, 5 vehicles on each. We started in 3<sup>rd</sup> place on our heat, based on the solo lap times. All vehicles finished without collisions or penalties, our vehicle finished in the 3<sup>rd</sup> place, 0.44 seconds (0.0871%) after the winner, which finished in 504.988 seconds. The average time was 506.7112 seconds since the remaining teams finished more than 3 seconds later. On the second heat, 3 of the 5 teams lost control or crashed, remaining with 7 teams for the finals, in total.

In the finals, our vehicle started in 5<sup>th</sup> place, and overtook 2 vehicles on the first lap. One team was disqualified due to crashing into another vehicle and the race was restarted with the 9 remaining laps. Our controller demonstrated collision-free and competitive driving capabilities and was able to keep 3<sup>rd</sup> place for a major part of the final race. 3 laps before the race ended, a vehicle tried to overtake our vehicle and entered our safety area. Our collision avoidance action exerted a high braking force, in the course of a corner, which caused our vehicle to deviate from the track. Therefore, we completed the race in the 6<sup>th</sup> place. The recording of the simulation race event is available at [28].

## VII. CONCLUSIONS

In this paper, we described our controller for the Indy autonomous challenge simulation race. Our main principles guiding our design were safety and conservative collision free navigation, while remaining competitive and efficient. The online planner plans a set of simple, dynamically feasible, maneuver candidates based on the point mass model exerted with a lateral bang-bang force. Each maneuver candidate is checked for collisions with the predicted future trajectories of the opponent vehicles, and the fastest maneuver is selected. The maneuver selection algorithm also takes into account the optimal race line and prevents fluctuation.

The trajectory following controller consists of a lateral and a longitudinal controller. The desired angular velocity is computed by the pure-pursuit algorithm; a proportional controller corrects the angular velocity by steering. The longitudinal proportional speed controller controls the desired velocity, which is computed based on the selected maneuver and blocking vehicles.

Our controller demonstrated effective and collision free driving in the IAC simulation race. Our controller also demonstrated competitive driving by finishing only 0.44 seconds after the winner which finished in 504.988 seconds on the semi-finals and maintaining 3<sup>rd</sup> place for a major part of the final race. We note that very few vehicles did not collide with any other vehicle; this emphasises the challenges of autonomous racing and the urgent need for additional research in complex autonomous driving.

## REFERENCES

- [1] "Indy autonomous challenge," 2021, <https://www.indyautonomouschallenge.com/>.
- [2] Ansys, "Ansys vrxperience driving simulator," 2021, <https://www.ansys.com/products/av-simulation/ansys-vrxperience-driving-simulator>.
- [3] "Ariel team passenger car autonomous driving," 2020, [https://youtu.be/J\\_26TnDg\\_sk](https://youtu.be/J_26TnDg_sk).
- [4] "Indy autonomous challenge rules," <https://www.indyautonomouschallenge.com/rules/year={2021}>.
- [5] "Formula student," 2021, <https://www.imeche.org/events/formula-student/about-formula-student/the-challenge>.
- [6] "roborace," 2021, <https://roborace.com/>.
- [7] J. Kabzan, M. I. Valls, V. J. Reijgwart, H. F. Hendrikx, C. Ehmke, M. Prajapat, A. Bühler, N. Gosala, M. Gupta, R. Sivanesan, *et al.*, "Amz driverless: The full autonomous racing system," *Journal of Field Robotics*, vol. 37, no. 7, pp. 1267–1294, 2020.
- [8] A. Liniger, A. Domahidi, and M. Morari, "Optimization-based autonomous racing of 1: 43 scale rc cars," *Optimal Control Applications and Methods*, vol. 36, no. 5, pp. 628–647, 2015.
- [9] F. Fuchs, Y. Song, E. Kaufmann, D. Scaramuzza, and P. Dürri, "Superhuman performance in gran turismo sport using deep reinforcement learning," *IEEE RA-L*, vol. 6, no. 3, pp. 4257–4264, 2021.
- [10] M. Jaritz, R. De Charette, M. Toromanoff, E. Perot, and F. Nashashibi, "End-to-end race driving with deep reinforcement learning," in *2018 IEEE ICRA*. IEEE, 2018, pp. 2070–2075.
- [11] S. Lefèvre, D. Vasquez, and C. Laugier, "A survey on motion prediction and risk assessment for intelligent vehicles," *ROBOMECH journal*, vol. 1, no. 1, pp. 1–14, 2014.
- [12] S. Ammoun and F. Nashashibi, "Real time trajectory prediction for collision risk estimation between vehicles," in *2009 IEEE 5th International Conference on Intelligent Computer Communication and Processing*. IEEE, 2009, pp. 417–422.
- [13] N. Deo and M. M. Trivedi, "Multi-modal trajectory prediction of surrounding vehicles with maneuver based lstms," in *2018 IEEE Intelligent Vehicles Symposium (IV)*. IEEE, 2018, pp. 1179–1184.
- [14] N. Li, E. Goubault, L. Pautet, and S. Putot, "Autonomous racecar control in head-to-head competition using mixed-integer quadratic programming," 2021.
- [15] P. Fiorini and Z. Shiller, "Motion planning in dynamic environments using velocity obstacles," *The International Journal of Robotics Research*, vol. 17, no. 7, pp. 760–772, 1998.
- [16] Z. Shiller, F. Large, and S. Sekhavat, "Motion planning in dynamic environments: Obstacles moving along arbitrary trajectories," in *Proceedings 2001 ICRA. IEEE International Conference on Robotics and Automation (Cat. No. 01CH37164)*, vol. 4. IEEE, 2001, pp. 3716–3721.
- [17] M. McNaughton, C. Urmson, J. M. Dolan, and J.-W. Lee, "Motion planning for autonomous driving with a conformal spatiotemporal lattice," in *2011 IEEE International Conference on Robotics and Automation*. IEEE, 2011, pp. 4889–4895.
- [18] K. Sun, B. Schlotfeldt, S. Chaves, P. Martin, G. Mandhyan, and V. Kumar, "Feedback enhanced motion planning for autonomous vehicles," in *2020 IEEE/RSJ International Conference on Intelligent Robots and Systems (IROS)*. IEEE, 2020, pp. 2126–2133.
- [19] S. Karaman and E. Frazzoli, "Sampling-based algorithms for optimal motion planning," *The international journal of robotics research*, vol. 30, no. 7, pp. 846–894, 2011.
- [20] J. M. Snider *et al.*, "Automatic steering methods for autonomous automobile path tracking," *Robotics Institute, Pittsburgh, PA, Tech. Rep.*, 2009.
- [21] C. Urmson, J. Anhalt, D. Bagnell, C. Baker, R. Bittner, M. Clark, J. Dolan, D. Duggins, T. Galatali, C. Geyer, *et al.*, "Autonomous driving in urban environments: Boss and the urban challenge," *Journal of Field Robotics*, vol. 25, no. 8, pp. 425–466, 2008.
- [22] X. Li, Z. Sun, D. Cao, Z. He, and Q. Zhu, "Real-time trajectory planning for autonomous urban driving: Framework, algorithms, and verifications," *IEEE/ASME Transactions on mechatronics*, vol. 21, no. 2, pp. 740–753, 2015.
- [23] "Tumftm global racetrajectory optimization," 2020, [https://github.com/TUMFTM/global\\_racetrajectory\\_optimization/](https://github.com/TUMFTM/global_racetrajectory_optimization/).
- [24] Z. Shiller and S. Sundar, "Emergency lane-change maneuvers of autonomous vehicles," *ASME*, 1998.
- [25] O. Amidi, "Integrated mobile robot control," *Carnegie Mellon University Robotics Institute, Tech. Rep.*, 1990.
- [26] T. A. Foundation, "Autoware.auto," 2021, <https://www.autoware.org/autoware-auto>.
- [27] "Autonomous head-to-head racing in the indy autonomous challenge simulation race," 2021, <https://youtu.be/f2nLufCZlbs>.
- [28] Ansys, "The ansys indy autonomous challenge simulation race," 2021, <https://youtu.be/gTjQ3sWdYh0>.